

1 **Title:** Kozak sequence libraries for characterizing transgenes across expression levels

2

3 **Running title:** Kozak libraries for functional genetics

4

5 **Authors:** Nidhi Shukla, Nisha D. Kamath, John C. Snell, Anna M. Bruchez, Kenneth A. Matreyek

6

7 **Affiliation:** Department of Pathology, Case Western Reserve University School of Medicine, Cleveland,

8 Ohio, USA

9

10 **Correspondence:** kenneth.matreyek@case.edu

11

## 12 **Abstract:**

13 Typical mammalian overexpression systems test protein sequence variants with little control  
14 over expression levels and steady-state protein abundances, hindering interpretations of how protein  
15 sequence and expression converge to yield phenotypic outcomes. We explored the translation initiation  
16 sequence, commonly referred to as the Kozak sequence, as a means to modulate protein steady-state  
17 abundance and cellular function. We performed sort-seq on a randomized library of the 6 nucleotides  
18 preceding the start codon, amounting to 4,042 sequences. Calibrating the scores revealed a ~100-fold  
19 range of protein steady-state abundances possible through manipulation of the Kozak sequence. We  
20 identified human germline variants with predicted expression-reducing Kozak substitutions in  
21 disease-associated genes. Modulating the cell surface abundance of the host cell receptor ACE2  
22 controlled the rate at which those cells became infected by SARS-like coronavirus spike pseudotyped  
23 particles. We demonstrated the potential of the approach by simultaneously testing Kozak libraries with  
24 a small panel of coding variants for ACE2 and STIM1. This approach lays the methodological  
25 groundwork for linking the causal relationships between protein sequence, abundance, and functional  
26 outcome.

27

## 28 **Introduction:**

29 Advancements in recombinant DNA technologies have aided development of cell-based assays  
30 characterizing how expression of transgenic coding sequences can impact cellular processes of  
31 interest. Unfortunately, most genetic experiments are performed in a binary fashion by simply toggling  
32 the existence or absence of a protein without major consideration toward controlling the amount of  
33 protein product being created per cell. We lack the experimental tools and knowledge needed to dial-in  
34 the precise levels of protein abundance and quantitatively observe the phenotypic outcomes.

35 For synthetically engineered systems, the Kozak sequence, also known as the eukaryotic  
36 translation initiation sequence (TIS), presents a convenient, genetically encoded method for modulating  
37 the steady-state abundance of a transgenic protein of interest. The Kozak sequence dictates the  
38 efficiency of cap-dependent protein translation by controlling the likelihood that a ribosome initiates at a  
39 particular ATG start codon encountered upon scanning from the 5' end of the mRNA (Kozak, 1981,  
40 1989). The Kozak sequence is generally regarded as the 6 nucleotides preceding the start codon,  
41 designated the -6 to -1 positions, as well as the first nucleotide following the start codon, designated the  
42 +4 position (Kozak, 1987), with other nearby nucleotides potentially contributing minor effects (Noderer  
43 *et al*, 2014).

44 Various studies have measured relative differences in efficiency between Kozak sequences  
45 across contexts. The first large-scale eukaryotic translation initiation dataset for Kozak sequences was  
46 created in PD-31 mouse pre-B lymphocytes, yielding a position weight matrix model for predicting  
47 translational score (Noderer *et al*, 2014). These scores were pseudo-quantitative, as the fold difference  
48 in protein amounts that could be inferred by comparing two scores was never defined. Other studies  
49 experimentally tested dozens to hundreds of Kozak sequences in yeast (Petersen *et al*, 2018),

50 *Drosophila* Kc167 cells (Acevedo *et al*, 2018), and human HEK 293T cells (Ambrosini *et al*, 2022).  
51 Despite these studies demonstrating the relative universality of Kozak sequence effects across  
52 eukaryotic cell backgrounds, we still lack a quantitative understanding for how any given pair of Kozak  
53 sequences differ in their resulting steady-state protein abundances.

54 We addressed this by creating a library of ~4,042 Kozak sequences modulating the expression  
55 level of the cell-surface protein ACE2 with the fluorescent protein mRFP670 fused to its cytoplasmic  
56 tail. These sequences were functionally assessed and given a calibrated abundance score, reflecting  
57 the mean-fluorescence intensity emitted by mRFP670 translated from that Kozak sequence. We used  
58 the ensuing scores to identify human germline variants that are potentially pathogenic due to reduced  
59 total amounts of particular disease associated protein. We varied ACE2 expression and tested the cells  
60 for their susceptibility to infection by virus particles dependent on ACE2 for entry into the cell. We also  
61 varied the expression amounts of STIM1, a protein involved in calcium signaling and cellular  
62 metabolism, and evaluated its effects on cell survival. This work demonstrates the potential of Kozak  
63 sequence modulation for learning how varying expression levels of different transgenic sequences or  
64 sequence variants correspond to functional output.

65

## 66 **Results:**

67

### 68 **Single-copy integration of a fluorescent protein Kozak library**

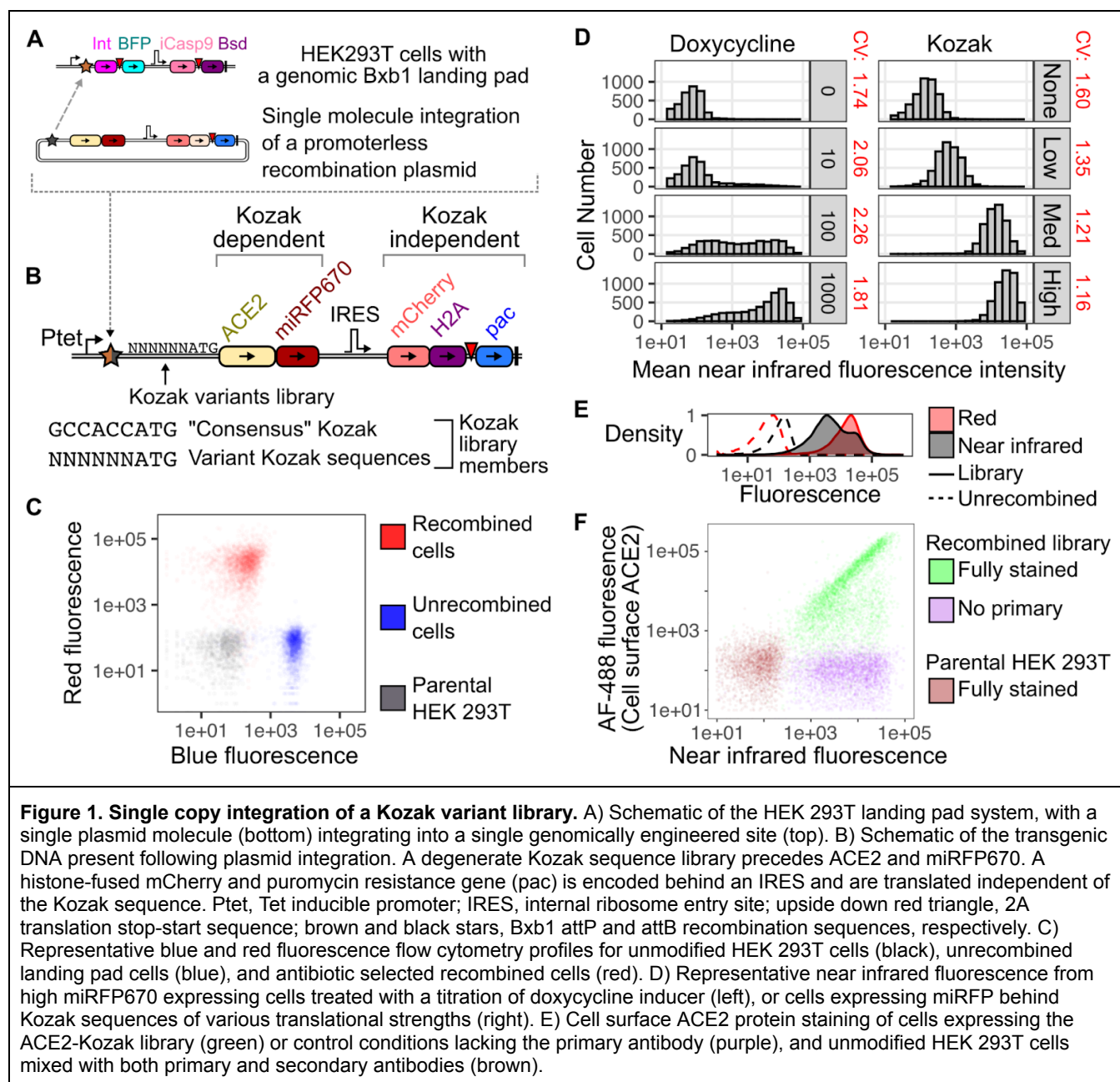
69 To perform our transgenic manipulations in cultured human-derived HEK293T cells, we  
70 harnessed targeted single-copy plasmid integration for transgenic overexpression, using a Bxb1  
71 landing pad cassette (Matreyek *et al*, 2017, 2020; Shukla *et al*, 2021). This system relies upon cells  
72 with a prior genomic integration of a single Bxb1 recombination site. The site is preceded by a  
73 Tet-inducible promoter, and followed by a cassette encoding a blue fluorescent reporter, positive and  
74 negative selectable markers, and the Bxb1 recombinase enzyme (**Fig 1A, top**). Expansion of clonal  
75 “landing pad” cells yields an isogenic line usable for integrating transgenic elements of interest.

76 Transfection of these cells with promoterless plasmids encoding the complementary Bxb1  
77 recombination site inserts a single plasmid molecule into the existing genomic landing pad site (**Fig 1A,**  
78 **bottom**). The previously promoterless transgene of interest is now behind the Tet-inducible promoter  
79 (**Fig 1B**), displacing and turning off expression of the prior DNA cassette. The recombined cells  
80 encoding the transgene of interest can be identified due to their loss of blue fluorescence and  
81 simultaneous gain of red fluorescence (**Fig 1C**). This system allows highly precise and stable  
82 transgenic expression compared to lentiviral transduction and transient transfection methods (Shukla *et*  
83 *al*, 2021). Since only a single molecule from a large pool of transfected plasmids becomes integrated,  
84 this transgenic expression method is compatible with single-cell library methods requiring strict links  
85 between cell genotype and phenotype (Matreyek *et al*, 2017, 2018, 2020).

86 Controlled modulation of steady-state transgenic protein expression is key to quantitative  
87 understanding of protein function, but generalizable strategies remain underdeveloped. Traditional  
88 approaches typically harness inducible promoters, such as the Tet-inducible promoter, where various  
89 concentrations of the chemical inducer doxycycline is used to achieve intermediate amounts of average  
90 protein expression at the population level. These methods are imprecise, as there is large cellular  
91 heterogeneity in protein abundance with intermediate inducer amounts (**Fig 1D, left**). The observed  
92 range of protein products achieved with intermediate chemical inducer concentrations are also not  
93 genetically encoded and cannot be measured using scalable molecular readouts such as high  
94 throughput DNA sequencing.

95 To achieve controlled modulation of protein steady-state abundance for our gene of interest, we  
96 focused on alterations to the eukaryotic translation initiation sequence. The Kozak sequence  
97 determines the rate of cap-dependent protein translation for a protein from a given mRNA,  
98 corresponding to a specific steady-state protein abundance setpoint (Noderer *et al*, 2014). We

99 confirmed that altering the Kozak sequence could tune steady-state protein abundance, and was  
 100 substantially more homogenous than with doxycycline titration, with more consistent coefficients of  
 101 variation across the expression range (**Fig 1D, right**).  
 102



103  
 104 As each Kozak-dictated steady-state abundance phenotype is genetically encoded, we used  
 105 DNA sequencing to identify cells with different levels of transgenic protein. To test the full range of  
 106 protein abundances within a single experiment, we created a library of Kozak sequence variants using  
 107 a primer with an internal degenerate segment encoding all possible nucleotides at the 6 positions  
 108 preceding the start codon. As alteration of the +4 position changes the protein coding sequence, we  
 109 kept this nucleotide invariant in our experiments, opting to maintain the wildtype nucleotide encoded by  
 110 the open reading frame. This library had a total potential complexity of  $4^6$  or 4,096 members (**Fig 1B,**  
 111 **bottom**).

112 To experimentally test the Kozak sequences, we created a promoterless recombination plasmid  
 113 encoding the cell-surface protein ACE2 with the near-infrared fluorescent protein miRFP670 fused to its  
 114 cytoplasmic C-terminus (**Fig 1B, top**). The coding region was immediately preceded by the degenerate

115 Kozak library nucleotides, which determined the translation rate and steady-state abundance of the  
 116 ACE2-miRFP670 fusion protein. To mark the genetically modified cells independently of the  
 117 Kozak-dependent translation products, the recombinant DNA construct also encoded the red  
 118 fluorescent protein mCherry fused to histone 2A, cotranslationally linked to the puromycin resistance  
 119 gene. These coding regions were preceded by an internal ribosome entry site, and thus translated  
 120 independently from the Kozak sequence (**Fig 1B, top**). The plasmid library was recombined into the  
 121 HEK 293T landing pad cells and enriched using sequential negative and positive selection to yield a  
 122 pure population of successfully modified, uniformly red fluorescent cells (**Fig 1E**). In contrast, these  
 123 cells had a wider range of near infrared fluorescence due to differing rates of cap-dependent translation  
 124 from the Kozak sequence library (**Fig 1E**).

125 We confirmed that miRFP670 intensity reflected the amount of ACE2 present on the cell surface  
 126 by staining the cells with an ACE2-targeting antibody followed by an Alexa Fluor-488 -conjugated  
 127 secondary antibody. We observed a clear linear relationship between near infrared fluorescence from  
 128 miRFP670 and green fluorescence from antibody staining (**Fig 1F**). This signal was specific for  
 129 overexpressed ACE2, as omission of either the primary or secondary antibody ablated green  
 130 fluorescence, and unmodified parental HEK 293T cells did not stain with the full combination of primary  
 131 and secondary antibody. We proceeded by using near infrared fluorescence intensity emitted by  
 132 miRFP670 to minimize unnecessary cell manipulation and costs during subsequent assay steps.

134 **Quantitating Kozak sequence impact on protein abundance**

135 We confirmed the range of protein abundances possible with the Kozak sequence library by  
 136 recombining plasmids encoding known strong and weak Kozak variants as controls (Noderer *et al*,  
 137 2014). The strong consensus Kozak (GCCACCATG) drove high miRFP670 fluorescence, while a weak  
 138 Kozak (TTATGGATG) yielded low miRFP670 fluorescence (**Fig 2A**). The cells within the library  
 139 population spanned these levels of fluorescence (**Fig 2A, green**), consistent with the library encoding a  
 140 diverse range of translational efficiencies possible with this approach.

141

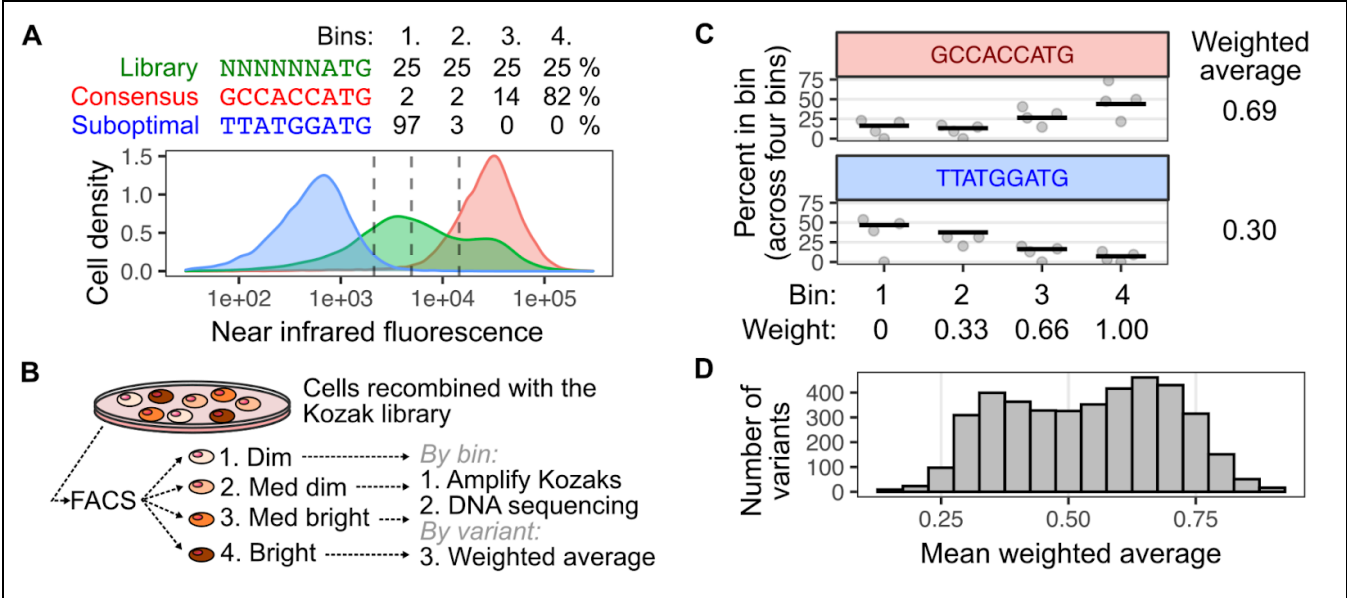


**Figure 2. 4-way sorting and sort-seq of the ACE2-Kozak cells based on near infrared fluorescence.** A) Cells encoding the ACE2-Kozak library (green) were compared to cells encoding ACE2 behind a weak (blue) or strong (red) translation Kozak sequences, and assessed for near infrared miRFP670 fluorescence using flow cytometry. The ACE2-Kozak library cell population was broken into quartile bins using threshold values (dotted lines), and the distribution of the control cells amongst the bins are shown as percentages. B) Schematic of the Sort-seq approach used to calculate steady-state abundance values corresponding to each Kozak variant. C) The distribution of DNA sequencing reads corresponding to the control Kozak sequences amongst the four bins for 5 replicate experiments, as well as the calculated mean weighted average corresponding to each sequence. D) Histogram of the mean weighted averages for all Kozak variants in the



dataset.

142

143

144 To characterize the steady-state protein abundance exhibited by each member of the library, the  
145 population of expanded library cells were separated into equally-populated quartiles using fluorescence  
146 activated cells sorting (FACS), creating four subsets of cells with different levels of fluorescence (**Fig**  
147 **2A, 2B**). The distribution of the cells across the four bins reflected the translation rate exhibited by that  
148 Kozak variant. For example, 97% of the TTATGGATG control Kozak cells were in the lowest quartile  
149 bin, with the remaining 3% in the second lowest bin, whereas 82% of the GCCACCATG control  
150 Kozak-containing cells were in the highest bin, with 14% found in the second highest bin, and the  
151 remaining 4% equally distributed between the lowest two bins (**Fig 2B**). The library was independently  
152 sorted into quartile bins on 4 separate occasions.

152

153 We performed high throughput DNA sequencing to quantitate the distributions of the library  
154 members (**Figure 2B**). Upon sorting, the cells from each quartile bin were grown for a week after which  
155 their genomic DNA was extracted. The DNA encompassing the Kozak sequence was amplified by  
156 polymerase chain reaction (PCR), and sequenced with Illumina high throughput DNA sequencing. The  
157 read counts for each Kozak sequence variant in each bin was divided by the total number of reads in  
158 that bin to convert each Kozak sequence variant into a frequency. By multiplying the frequencies with a  
159 weight value specific for each bin (ranging from 0 to 1; see **Fig 2C**), each Kozak sequence variant was  
160 given a weighted average value.

160

161 This process was repeated for each sorted replicate, and a mean weighted average was  
162 calculated for each variant across the replicate experiments. We obtained weighted average scores for  
163 4,042 variants. The variants largely spanned the range from roughly 0.13 to 0.91 (**Fig 2D**). The  
164 aforementioned strong and weak Kozak control variants exhibited weighted averages of 0.69 and 0.30,  
165 respectively (**Fig 2C**).

165

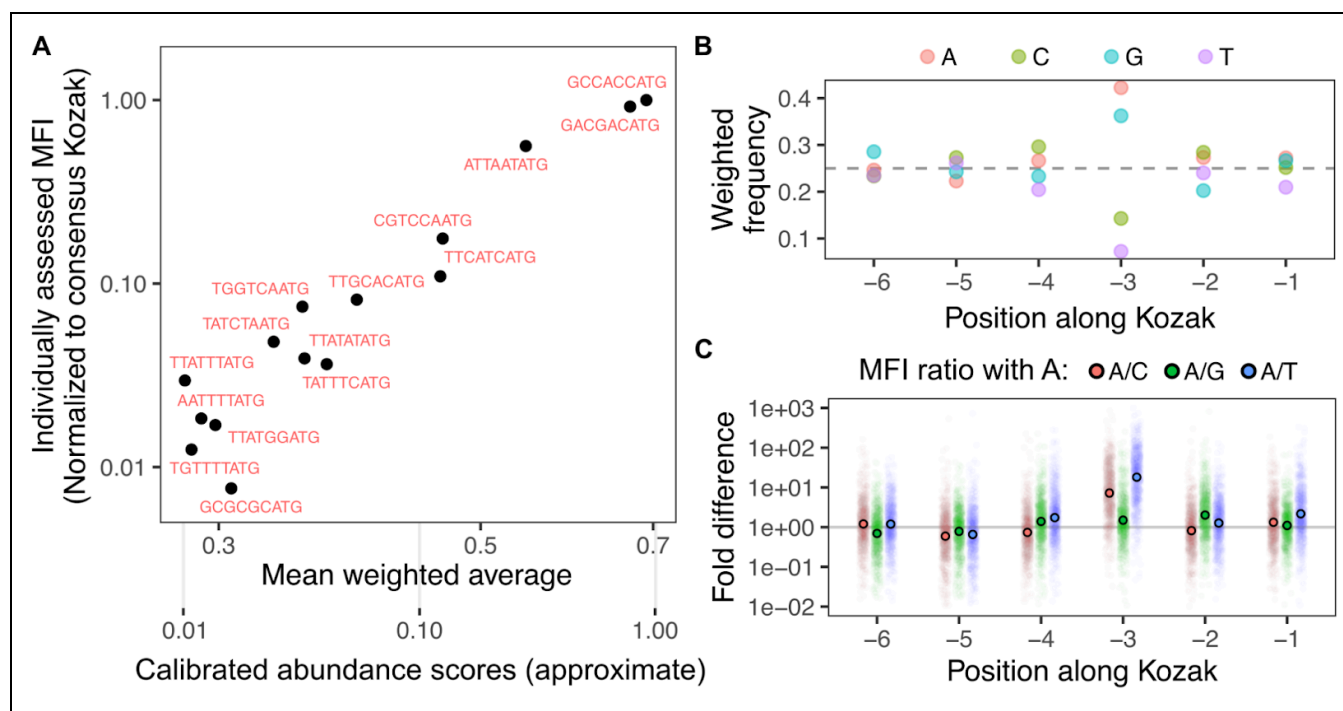


**Figure 3. Calibration and analysis of Kozak sort-seq scores.** A) Comparison of the mean weighted average of each Kozak sequence (x-axis, top) from sort-seq analysis, as well as the individually assessed mean fluorescence intensity of cells encoding each Kozak through analytical flow cytometry (y-axis), normalized to the GCCACC consensus Kozak sequence. Based on this calibration curve, an estimated MFI was calculated based on the sort-seq values (x-axis, bottom). B) Position weight matrix denoting individual nucleotide contributions to overall Kozak sequence effects on calibrated abundance score. C) Positional impacts of various nucleotides on translational efficiency, shown as fold differences compared to that from A at each position. Small colored circles denote individual variants from the library, while the larger

166

167 While these weighted averages can distinguish the effects conferred by different Kozak  
168 sequences, they cannot be directly used to interpret fold differences in protein steady-state  
169 abundances. We thus calibrated our weighted average values to the mean fluorescence intensity (MFI)  
170 exhibited by miRFP670 when tested individually. We chose a panel of 16 Kozak sequences spanning  
171 the range of weighted scores, created constructs specific for each sequence, generated clonal  
172 populations of cells with each construct, and assessed the resulting cells for miRFP670 fluorescence  
173 using flow cytometry. The resulting MFIs exhibited high correlation with the mean weighted averages  
174 (Pearson's  $r^2 = 0.92$ , Spearman's  $\rho^2 = 0.86$ ; **Fig 3A**). We used regression to calculate an estimated MFI  
175 for each variant scored in the library, and refer to these values as “calibrated abundance scores”.

176 These values enabled the generation of new quantitative magnitude estimates for known  
177 positional effects within Kozak sequences. As expected, the position weight matrix values showed that  
178 adenine and guanine were highly favored at position -3 (**Fig 3B**). The importance of this position is well  
179 known (Noderer *et al*, 2014; Kozak, 1986, 1987), but our MFI-scaled dataset yielded alternative ways to  
180 measure this effect. For every sequence, we calculated the fold difference in MFI-calibrated score when  
181 A was encoded at a given position, compared to C, G, and T (**Fig 3C**). On average, we found that an A  
182 at the -3 position yielded 1.3-fold more protein abundance over G, 5.2-fold over C, and 13.4-fold over T.  
183 In contrast, the effects at position -1 were comparatively minor, with an A yielding 1.1-fold more protein  
184 abundance over G, 1.3-fold over C, and 2.1-fold over T.

185

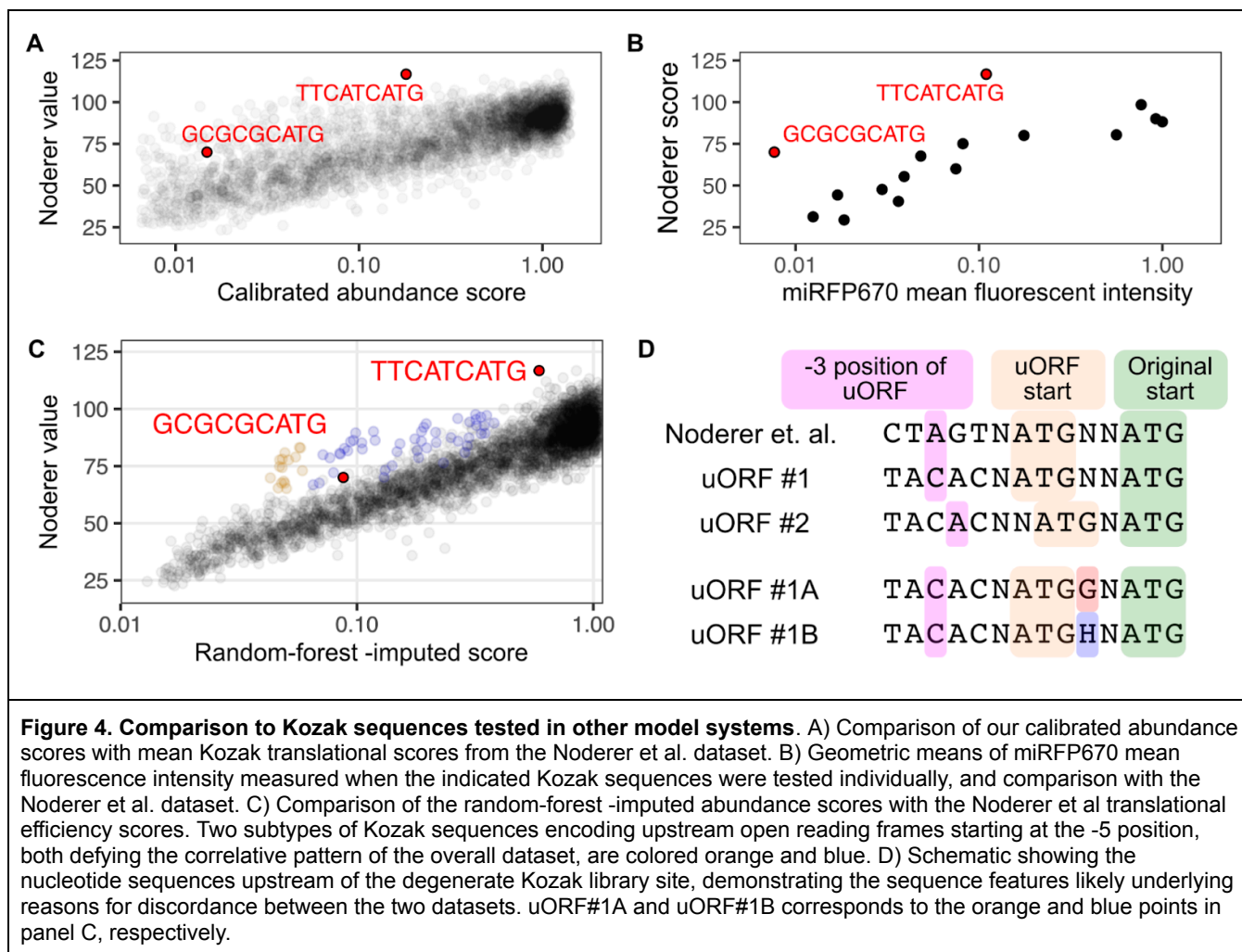
#### 186 **Comparison of scores across data sources**

187 We compared our dataset of calibrated abundance scores to the Noderer *et al*. dataset. Their  
188 reported scores were outputs of a position weight matrix model based on their experimentally  
189 measured data (Noderer *et al*, 2014). Their modeled scores correlated with our calibrated abundance  
190 scores (Pearson's  $r^2 = 0.56$ , Spearman's  $\rho^2 = 0.6$ ; **Fig 4A**), and the correlation improved when the  
191 logarithm of our calibrated abundance scores were used (Pearson's  $r^2 = 0.67$ ). Thus, their scores,  
192 ranging from 11 to 161, were logarithmically proportional to more traditional measurements of relative  
193 protein abundance such as with flow cytometry.

194 Despite the overall correlation, there were some discrepancies between the datasets. This was  
195 particularly evident for “GCGCGCATG” and “TTCATCATG, as these were also present in our panel of  
196 individually tested sequences (**Fig 4B**). We suspected that the Noderer *et al*. scores being reported as  
197 position weight matrix output values may have contributed to the discrepancies between our two  
198 datasets. We created a similar set of modeled output values using a random forest machine learning  
199 model on the MFI-calibrated scores yielded by our assay. We observed model outputs that were highly  
200 correlated with the Noderer *et al* values (Pearson's  $r^2 = 0.85$ , Spearman's  $\rho^2 = 0.75$ ). The improved  
201 correlation of the random forest model output, as compared to our calibrated scores, suggest that the  
202 models converged on similar Kozak sequence properties.

203 A subset of data points were outliers exhibiting higher Noderer scores than predicted by our  
204 model (**Fig 4C, orange and blue points**). The biggest discrepancies were from sequences introducing  
205 an ATG start codon prior to the intended protein start site, creating out-of-frame upstream open reading  
206 frames (uORFs) at the -5 position, with those encoding G at the +4 position the most extreme (**Fig 4C**).  
207 A G at the +4 position is predicted to enhance translation initiation of the uORF (Noderer *et al*, 2014),  
208 which likely causes greater disruption of the downstream coding ORF than other nucleotides at the +4  
209 position. The discrepancy between the models is likely attributable to there being a weaker G  
210 nucleotide in the -3 position of the Noderer *et al*. constructs, while our constructs encode the  
211 translation-enhancing A nucleotide (**Fig 4D**). Thus, these scores can also inform how competition with  
212 uORFs impact the steady-state abundance of transgenically encoded proteins.

213



214

215 We assessed the generality of these effects by comparing our scores to other studies testing  
 216 Kozak sequence changes at smaller throughput across model systems. Our scores correlated with 244  
 217 values derived from lentivirally transduced HEK 293T cells (Pearson's  $r^2$ : 0.55, Spearman's  $\rho^2$ : 0.56)  
 218 (Ambrosini *et al*, 2022) (**Supplementary Fig 1**). Our scores also correlated with a set of 50 constructs  
 219 tested in insect cells (Pearson's  $r^2$ : 0.74, Spearman's  $\rho^2$ : 0.77) (Acevedo *et al*, 2018). Thus, our scores  
 220 are likely to be applicable when modulating Kozak sequences across eukaryotic cells.

221

## 222 Germline Kozak variants in disease genes

223 We applied our calibrated scores to identify human germline variants that may cause disease  
 224 through reduced steady-state abundance of key proteins. We identified Kozak sequence variants  
 225 reported in ClinVar, a repository of largely germline genetic variations and their clinical significance  
 226 observed through clinical laboratory genetic testing of patients (Landrum *et al*, 2018). We found 1,826  
 227 Kozak variants in ClinVar that were within the 6 nucleotide stretch scored within our dataset. Roughly  
 228 5% of these were predicted to reduce protein abundance by at least 4-fold (**Fig 5A**).

229 We focused on the ACMG73, which is a collection of genes most important for clinical genetics  
 230 (Miller *et al*, 2023). We found 18 Kozak variants in these genes expected to reduce protein abundance  
 231 by at least 5-fold (**Fig 5B**; red points). Kozak variants in tumor suppressor genes were particularly  
 232 notable, as the presence of even one variant allele encoding a protein with reduced activity can result in  
 233 increased cancer predisposition. This included multiple DNA repair genes listed in the ACMG73, such  
 234 as BRCA1, MSH6, PMS2, and TP53 (**Fig 5B**).

235 The variants with the greatest magnitude reductions generally encoded uORFs, such as the  
 236 -4A>T variant of BRCA1 and the -2C>G variant of PMS2 (**Fig 5C**). The functional impact of this PMS2

variant was recently shown to exhibit significantly reduced translation in an alternative assay system (Matoy *et al*, 2024). Impactful substitutions of the -3 position were also observed, such as -3G>T variants of MSH6 and VHL, and a -3A>T variant of KCNH2. There were also variants in established disease genes not included in the ACMG73, such as RAD51C. As these variants are currently listed as “variants of unknown significance”, the functional results from our dataset may be helpful in future reclassification of these types of variants (Starita *et al*, 2017).

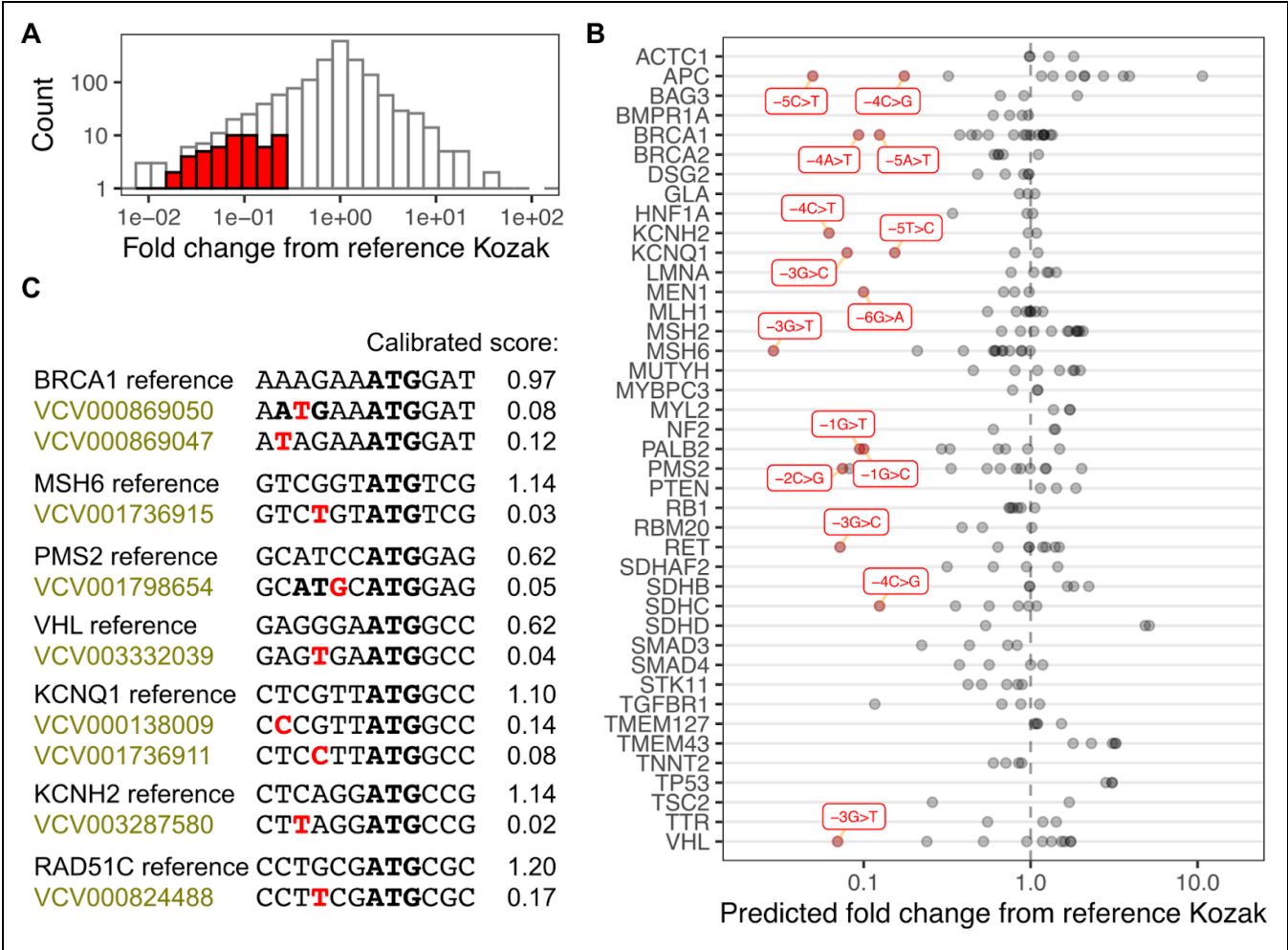


**Figure 5. Germline Kozak variants in disease genes.** A) A histogram of Kozak sequence variants listed in ClinVar, with high confidence scores causing greater than 4-fold decreases to calibrated abundance score relative to the reference sequence colored as red bars. B) Plot denoting protein relative fold abundance changes predicted for various ClinVar entries of Kozak germline variants, for genes found in the ACMG73. High confidence scores exhibiting greater than 5-fold reduction to calibrated abundance score from the reference sequence are labeled and colored in red. C) Examples of various disease-associated genes, their reference Kozak sequences, and single nucleotide variants observed as entries in ClinVar. The single nucleotide variant is colored red, and initiator methionine codons are in bold. Labels for variants of uncertain significance are colored gold.

**Gradations of functional output with Kozak libraries**

With the relative steady-state protein abundances defined for each Kozak sequence, we used the Kozak sequence library in cultured cell assays to characterize how different protein abundance levels impact cellular activity. Using a handful of Kozak sequences, we previously showed that the cell surface abundance level of ACE2 can impact virus entry and rates of antibody-mediated neutralization of SARS-CoV-2 spike pseudotyped virus particles (Shukla *et al*, 2021; Farrell *et al*, 2022; Roelle *et al*, 2022). We used the Kozak library driving ACE2-miRFP670 expression to assess how virus infectivity changes across the full range of expression levels.



253 To assess how ACE2 cell surface abundance correlated with infectivity, we performed a  
 254 multiplexed infection assay with our ACE2 Kozak library cells (Shukla *et al*, 2024) (**Fig 6A**). We mixed  
 255 the cells with lentiviral particles encoding EGFP and the hygromycin resistance gene, but coated with  
 256 SARS-CoV spike, SARS-CoV-2 spike, or the unrelated glycoprotein from vesicular stomatitis virus  
 257 (VSV-G). Unlike the coronavirus spike proteins, VSV-G uses the ubiquitously expressed low density  
 258 lipoprotein receptor for cell entry rather than ACE2 (**Fig 6A**). After green cells were observed, genomic  
 259 DNA from a subsample of cells were collected and stored. The remaining cells were treated with  
 260 hygromycin to remove uninfected cells, and ensure that only genomic DNA from infected cells would be  
 261 retained. The Kozak sequences were amplified, sequenced, and tallied before and after selection. An  
 262 enrichment ratio was calculated for each Kozak sequence to determine their relative rates of infection  
 263 by each pseudotyped virus (**Fig 6A**).  
 264 Visualizing the enrichment ratio relative to our previously ascertained abundance values  
 265 revealed how ACE2 cell surface amounts corresponded to infection (**Fig 6B**). As expected,  
 266 pseudotyped viruses coated with VSV-G infected all cells equally, regardless of the level of ACE2  
 267 abundance (**Fig 6B**). In contrast, infectivity of the SARS-CoV and SARS-CoV-2 spike pseudotyped  
 268 viruses correlated with the level of ACE2 abundance, and were nearly identical when compared to each  
 269 other (**Fig 6B, right**).  
 270

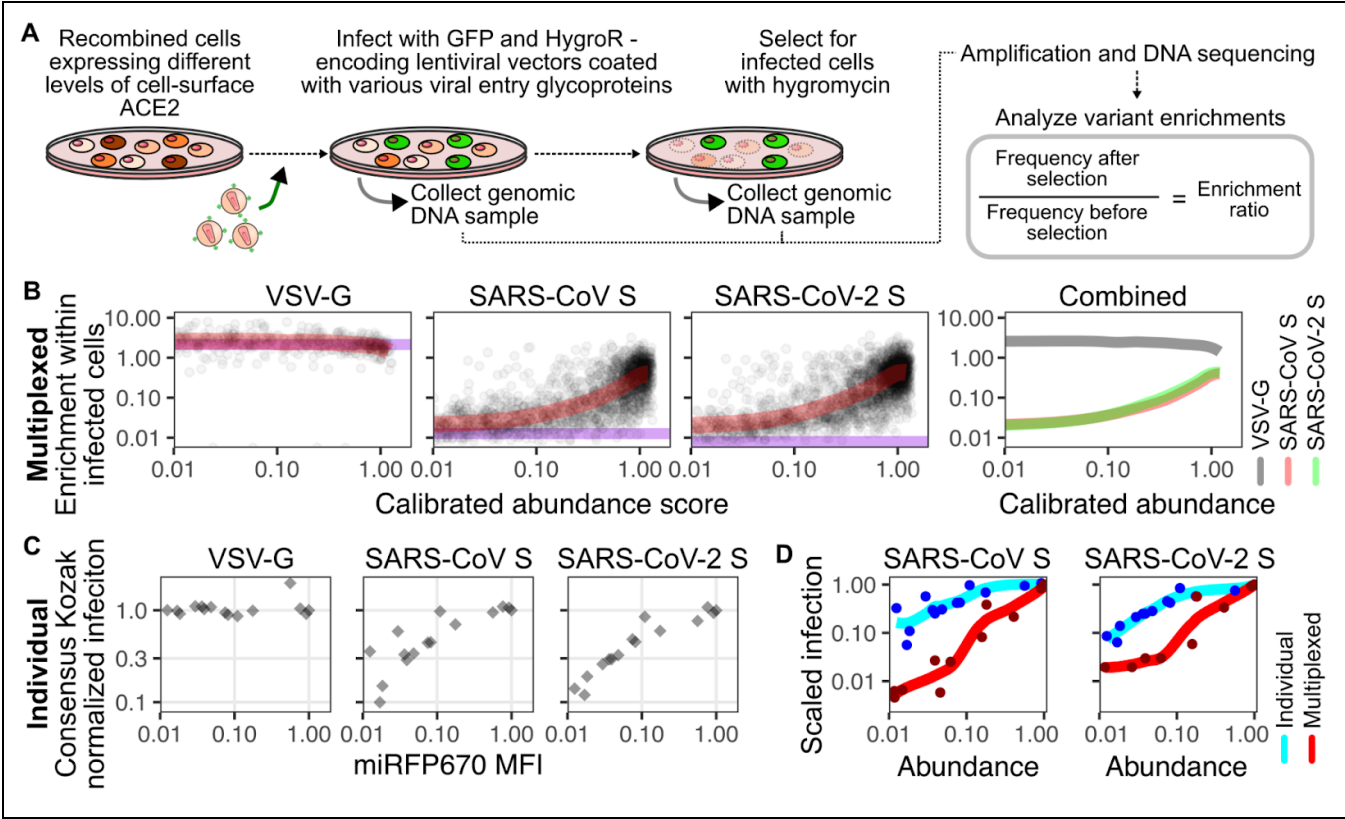


**Figure 6. ACE2 expression level impacts on SARS-CoV spike-mediated infection.**  
 A) Work-flow diagram describing key physical and computational steps for the multiplex infection assay readout. B) Scatterplots of pseudotyped virus infectivity as a function of calibrated abundance scores. The semi-translucent red lines denote a LOESS fit to the points. The plot to the rightmost column overlay these LOESS curves. The horizontal purple line denotes the infectivity of template plasmid, which encodes a null ACE2 sequence lacking its start codon. C) Scatterplots of pseudotyped virus infectivity as a function of miRFP670 fluorescence of a set of clonally tested Kozak sequences. D) Scatterplot overlays of the same set of Kozak sequences shown in panels 6B and 6C, with normalized infection score as a function of protein abundance. The LOESS fit colors denote the two different assay types compared.

271  
 272 We next compared whether the relationship between ACE2 abundance and likelihood of  
 273 pseudotyped virus entry changed depending on the assay format. We thus infected the same 15 clonal  
 274 cell lines of varying Kozak strengths used to create the MFI calibration scores with the pseudotyped

viruses (**Fig 6C**). When the results from each assay format were scaled to the consensus Kozak, we observed clear differences imposed by ACE2 expression on target cell infection, depending on whether the assay was performed with homogeneous or heterogeneous cell mixtures (**Fig 6D**). For example, ACE2 Kozak sequences that had calibrated abundance scores of 0.1 exhibited 10-fold less infection than ACE2 behind a consensus Kozak when tested as a pooled library, while the same sequences when tested as individual, homogenous cultures exhibited no differences to infectivity (**Fig 6D**). These results highlight discrepancies in biological assays that can only be identified when performing the assay in a pooled manner.

283

284 **Modulating protein sequence and abundance**

285

Simultaneous modulation of protein sequence and steady-state abundance levels would vastly improve our understanding of the functional impacts of coding sequence changes. Our Kozak library experiments showed that the -6 position has little impact on determining ensuing protein steady-state abundance, so we explored rendering this nucleotide invariant to serve as a genetically encoded identifier for marking which construct variant is being sequenced, like a standard nucleotide barcode. We found that all of the remaining library members still spanned the full 100-fold range of abundance, regardless of which nucleotide base was fixed at the -6 position (**Fig 7A**).

292

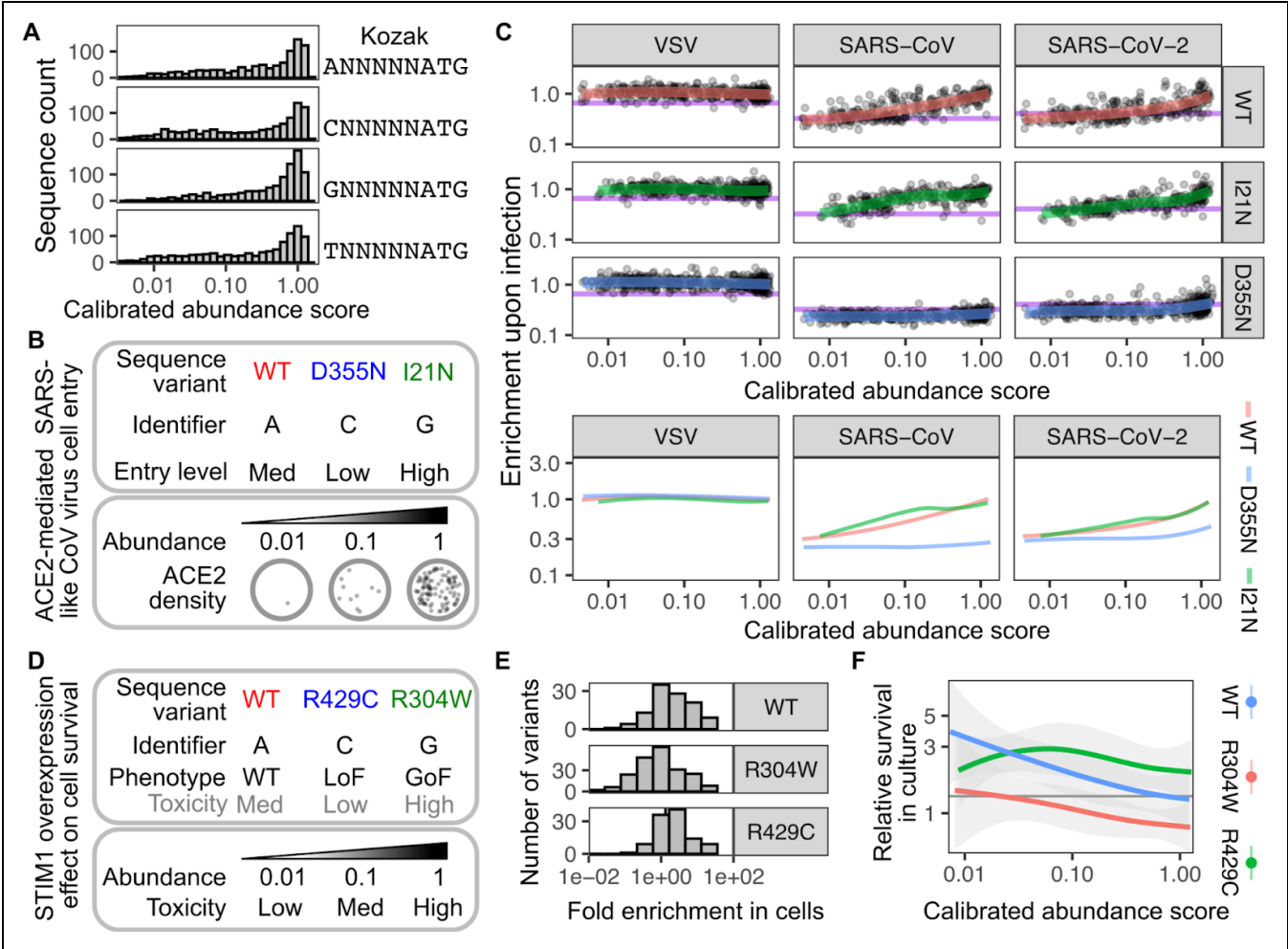


**Figure 7. Results of simultaneously modulating protein sequence and expression.**

A) Histograms of calibrated scores when the -6 Kozak nucleotide is left invariant. B) Schematic demonstrating the ACE2 sequence variants, their nucleotide identifiers, and their anticipated infection phenotypes (top), as well as a visual depiction of 100-fold receptor density differences expected on a two-dimensional plane, mimicking cell surface density (bottom). C) Scatterplots of pseudotyped virus infectivity as a function of calibrated abundance scores of ACE2 variants. The semi-translucent red, green, and blue lines denote LOESS fits to the points. The scatterplots in the bottom row overlay these LOESS curves. The horizontal purple line denotes the infectivity of template plasmid, which encodes a null ACE2

sequence lacking its start codon. D) Schematic demonstrating the STIM1 sequence variants, their nucleotide identifiers, and their anticipated cell toxicity phenotypes (top), as well as a key denoting how STIM1 abundance level is expected to correspond to cell toxicity (bottom). E) Histograms showing the distribution of cell survival scores, separated by STIM1 variant. F) Overlaid LOESS curves fitting data-points denoting cell survival as a function of STIM1 calibrated abundance score.

293

294 To test this concept, we tagged the WT ACE2 Kozak library construct with A, while the known  
295 loss-of-binding ACE2 variant D355N was tagged with C, and a minor infection-enhancing variant I21N  
296 was tagged with G (**Fig 7B**). The ensuing cells were pooled, infected with one of three pseudotyped  
297 viruses, selected with hygromycin, sequenced, and computationally separated for analysis using the  
298 nucleotide identifier. Like earlier, we observed no WT ACE2-dependent enhancement to infection by  
299 VSV-G pseudotyped virus, but dose-dependent enhancement to infection for viruses coated with  
300 SARS-CoV or SARS-CoV-2 spike (**Fig 7C, red**). D355N ACE2 cells in the same well were poorly  
301 infectable, although they showed a slight uptick to infectivity at the highest abundance levels,  
302 suggesting that high overexpression can partially functionally compensate for poor binding (**Fig 7C,**  
303 **blue**). In contrast, I21N ACE2 cells exhibited enhanced infectivity relative to the other variants,  
304 particularly for SARS-CoV spike (**Fig 7C, green**).

305 We next applied this strategy to STIM1, which is involved in sensing depletion of endoplasmic  
306 reticulum calcium to conformationally rearrange and trigger influx of cytoplasmic calcium from the  
307 extracellular environment. We recently demonstrated that the myopathy-causing gain-of-function  
308 R304W variant, and the immunodeficiency-associated R429C variant, exhibit contrasting effects on  
309 cell-growth and survival when overexpressed in HEK 293T landing pad cells (Kamath & Matreyek,  
310 2025). Kozak libraries for these STIM1 variants were tagged by invariant nucleotide identifiers and  
311 expressed in HEK 293T landing pad cells (**Fig 7D**). DNA was amplified prior to and following  
312 recombination and growth in culture, sequenced with high throughput DNA sequencing, and analyzed  
313 for relative cell survival over time. Overall, cells expressing R304W depleted in culture relative to WT,  
314 while cells with the R429C variant became enriched (**Fig 7E**).

315 Separation of the variants by relative expression levels revealed dose-dependent contributions  
316 to variant effect. R304W caused overt toxicity of this variant regardless of the level it was expressed.  
317 Increasing dosage of WT STIM1 protein abundance caused reduced survival, indicative of cellular  
318 dysregulation occurring through gross overexpression (**Fig 7F**). Despite its overall high level of cell  
319 survival, R429C yielded a potentially complex curve of dose-based effect. Our results demonstrate that  
320 simultaneous modulation of protein sequence and steady-state abundance are a potentially valuable  
321 approach to understanding the impacts of protein coding variants, either as a quantitative assay itself or  
322 as an unbiased means for assay optimization.

323

## 324 Discussion:

325 In this work, we provide improved measurement of the changes to steady-state protein  
326 abundance possible through modulation of the Kozak sequence. This information improves  
327 retrospective observational analysis, as it aids in functional interpretation of existing genetic variation.  
328 We furthermore demonstrate that synthetic variation of the Kozak sequence with nucleotide libraries  
329 can be leveraged to tie differences in protein abundance with functional effect, a relationship not  
330 captured in most cell-based assays.

331 The wealth of additional existing information about the Kozak sequence helps to infer the  
332 generality of our results. We observed high correlation between our data and the existing gold-standard  
333 (Noderer *et al*, 2014). As this dataset was collected in murine cells, this suggests that our results will  
334 likely apply across mammals. Our data also correlated, albeit to a reduced extent, with a smaller  
335 dataset collected in insect cells (Acevedo *et al*, 2018).

336 We observed improved correlation with the gold-standard dataset when values imputed from a  
337 model trained on our calibrated abundance scores were used. This may be attributable to more than

one factor. Our sort-seq workflow exhibits experimental variability, error from which will likely impact individual experimental measurements more than individual predictions from a computational model based on that data. Furthermore, neither computational model likely accounts for sequences with higher-order outlier effects, such as “GCGCGCATG”, which was predicted by both models to cause higher steady-state protein abundance than experimentally determined. To limit any associated concerns, we chose to perform all subsequent analyses with our calibrated abundance scores.

We demonstrate the utility of the Kozak scores for data interpretation by identifying clinically observed Kozak sequence germline variants predicted to reduce steady-state protein abundance greater than 4-fold, in genes known to potentially cause disease when the ensuing protein function is reduced. There are a handful of examples of Kozak sequence changes being associated with human disease, such as a -6G>C change in  $\beta$ -globin exacerbating thalassemia presentation in an Italian family when present as a compound heterozygous with other thalassemia promoting alleles (De Angioletti *et al*, 2004), and a different -6G>C change in the Kozak sequence of the transcription factor GATA4 which was associated with atrial septal defects in a Dutch family (Mohan *et al*, 2014).

While we looked specifically at predicted expression-reducing Kozak germline variants in clinically actionable genes, expression-enhancing Kozak variants may also dysregulate physiology in certain genes. Somatic Kozak variants may also be examined, such as the tumor-associated Kozak variants that may be contributing to oncogenesis (Noderer *et al*, 2014). By capturing how Kozak sequence relates to protein-steady state abundance, our dataset may aid future development of more intricate models relating genomic sequence to functional effect, such as expression quantitative trait loci. This information may also aid therapeutic reversion of disease-associated Kozak variants through base- or prime-editing of endogenous loci (Ambrosini *et al*, 2022; Xie *et al*, 2023).

Cells naturally regulate functional output through programmed changes to protein synthesis, such as during differentiation (Kristensen *et al*, 2013). We leveraged this overall strategy of modulating protein synthesis to enact functional changes at the cellular level, albeit through targeted perturbation of the rate of translation initiation. This method is experimentally convenient since it only requires programming of a small stretch of nucleotides, easily introduced with an oligonucleotide primer during PCR. Regulation of protein translation initiation is the final step of protein expression, and is thus tightly linked to protein function. This likely contributes to our observation that cell-to-cell variability in protein expression was drastically reduced with programmed control of translation initiation, in contrast to the drastically increased variability observed with transcriptional control of the doxycycline-inducible promoter.

Our calibrated abundance scores established in this work also provide reference values for future multiplexed genetic assays measuring the relationship between protein abundance and cellular effect. The concept of reactant modulation is also well established for *in vitro* biochemical experiments, which often leverage titration of purified components, but we have lacked the tools to perform similar modulation in cell based experiments. This is particularly important for proteins that exhibit membrane localization and/or multimerization, as such situations often involve binding avidity which is typically difficult to re-create authentically with isolated components *in vitro*. The binding interactions underlying virus entry can be an example of this, where cell-based assays with viral particles can reveal functional interactions between virus and host membrane glycoproteins that are not observed when tested *in vitro* as monomeric subunits (Shukla *et al*, 2021). Despite the D355N variant abrogating binding or infection with all previously tested assay formats (Shukla *et al*, 2021; Ren *et al*, 2022; Bhattacharjee *et al*, 2021), we still observed a slight uptick to SARS-CoV-2 spike pseudotyped virus infection conferred by ACE2 D355N expressed at the highest levels, suggesting that binding avidity is still counteracting the drastic loss of binding affinity conferred by this mutant.

Affinofile cells, which use small molecules as inducers to modulate the cell surface expression of CXCR4 and CCR5, have been a valuable tool for HIV research (Johnston *et al*, 2009), and our system furthers these capabilities. With Kozak-determined translation regulation being genetically



387 encoded, it allows for multiplex genetic approaches not possible through chemical induction.  
388 Transcriptional regulation used in the Affinofile system likely mimics the characteristics of our own  
389 doxycycline titration experiments, where inducer titration modulates mean protein expression at the  
390 population level while exhibiting much higher single-cell heterogeneity than our translational regulation  
391 system. Since our experiments were performed with HEK293T landing pad cells purposefully  
392 engineered to accept diverse cDNA cargos, additional protein interactions could easily be tested by  
393 targeted genomic integration of the relevant coding sequences, requiring vastly less cell engineering  
394 than other non-modular methods.

395 Our work highlights how the same functional assay can differ depending on whether each  
396 sequence is being tested in isolation as a homogenous population or as a pool multiplex experiment.  
397 Lentiviral particles coated with spike glycoprotein and entering host cells via interactions with ACE2  
398 exhibited a maximum limit to the dose-dependent increase to infection when each sample was tested  
399 individually as homogenous cultures, while this limit was not encountered when the assay was  
400 performed as a pool library. For the many real-life cases where phenotypic variation is occurring in an  
401 otherwise mixed pool of cells, it is possible that the multiplexed format will capture information in a  
402 manner more relevant to the underlying biology under investigation than the traditional arrayed format.

403 Our results point to the vast potential of simultaneously modulating protein sequence and  
404 abundance level when performing the cell based functional assays. We could have tested the three  
405 variants of ACE2 and STIM1 as separate Kozak libraries, but the fully-pooled format possible by using  
406 the -6 Kozak position as the coding variant identifier allowed us to mitigate batch effects and similar  
407 sources of experimental error. Even larger sequence-abundance multiplex assays of variant effect will  
408 necessitate additional barcoding capacity through larger nucleotide identifier sections, but readily  
409 achievable through existing molecular methods.

410 Regulation of protein translation initiation is a convenient and effective method for functional  
411 regulation, both in natural and synthetic contexts. Our work provides calibrated, quantitative values that  
412 improve interpretation of naturally occurring variants that may contribute to disease. Our experiments  
413 also establish the methodological framework for genetic control of protein translation as a molecular  
414 rheostat, wherein control of signal intensity can be combined with libraries of protein coding variants to  
415 enable understanding of the combinatorial intersection of protein sequence and abundance to cellular  
416 function.

417

## 418 **Materials and Methods:**

419

### 420 **Cell culture**

421 The generation of the HEK 293T LLP-Int-IRES-iCasp9-Blast Bxb1 landing pad cell line used in  
422 this work was previously described (Shukla *et al*, 2021). Cells were cultured in D10 medium  
423 (Dulbecco's modified Eagle's medium supplemented with 10% fetal bovine serum, 100 U/mL penicillin,  
424 and 0.1 mg/mL streptomycin). To induce transcription from the landing pad promoter, the cells were  
425 switched to D10X medium (D10 supplemented with 2 µg/mL doxycycline). Long-term passaging of  
426 unrecombined landing pad cells was performed with D10X medium supplemented with 20 µg/mL  
427 blasticidin, to select against cells that silence the landing pad locus. All cell detachment steps were  
428 performed with a 0.25% solution of Trypsin-EDTA (Corning, 25-053-CI).

429

### 430 **Recombinant DNA construction**

431 Recombinant plasmid DNAs were generated using Gibson Assembly. DNA fragments were  
432 amplified from 40 ng of plasmid DNA using 0.33 µM each of forward and reverse primers and 2X Kapa  
433 HIFI HotStart ReadyMix. The PCR conditions included an initial denaturation at 95°C for 5 minutes,  
434 followed by nine cycles of 98°C for 20 seconds, 65°C for 15 seconds, and 72°C for 8 minutes,  
435 concluding with a final extension at 72°C for 5 minutes. The resulting amplicons underwent DpnI  
436 digestion with 20 U of enzyme at 37°C for 2 hours to remove template DNA. Reactions were purified  
437 using a Zymo clean and concentrator kit, and 2 µL of the eluted product was combined with 2 µL of  
438 GeneArt Gibson Assembly enzyme mix (Thermo Fisher, A46629). The mixture was incubated at 50°C  
439 for 30 minutes before transformation into chemically competent *E. coli* DH10β cells, which were  
440 subsequently plated on LB-agar supplemented with 150 µg/mL ampicillin and incubated overnight.  
441 Colonies were screened by overnight growth in LB media containing 150 µg/mL ampicillin, followed by  
442 plasmid isolation using a GeneJet Plasmid Miniprep kit (Thermo Fisher, K0503). The presence of the  
443 desired transgene was verified in each candidate clone through Sanger sequencing, with whole  
444 plasmid sequencing performed on all selected clonal variants utilized in the study.

445 To generate the ACE2 Kozak libraries, Gibson assembly reactions were prepared in 30 µL  
446 volumes consisting of 40 ng of template DNA, 0.33 µM of the designated primer pair, 10 µL of  
447 nuclease-free water, and 15 µL of Kapa HiFi HotStart ReadyMix polymerase. For each library, four PCR  
448 reactions were prepared. The assembled plasmid products were pooled and purified with a Zymo clean  
449 and concentrator kit. 5 µL of the cleaned product was combined with 5 µL of GeneArt Gibson assembly  
450 master mix and incubated at 50°C for 60 minutes. The assembled plasmid product was purified with a  
451 Zymo clean and concentrator kit and eluted in 10 µL of nuclease-free water. Cleaned PCR products  
452 were electroporated into *E. coli* DH10β cells (New England BioLabs, C3019I). Each bacterial pellet  
453 corresponding to a library was resuspended in 1 mL of sterile LB medium, and appropriate volumes (8,  
454 16, 32, and 64 µL) were plated on LB-agar plates containing ampicillin to assess colony-forming units.  
455 The remaining bacterial culture was used to inoculate 200 mL of LB with 150 µg/mL ampicillin, followed  
456 by plasmid purification using a NucleoSpin Plasmid kit (Macherey-Nagel, NC0389395). To confirm  
457 successful construction, 6-8 bacterial colonies from LB plates were picked randomly, purified using the  
458 GeneJET Miniprep kit, and sequence-verified by Sanger sequencing using an Applied Biosystems 3730  
459 Genetic Analyzer.

460 The G868A\_AttB\_[mutATG]ACE2-miRFP670\_IRES\_mCherry-H2A-P2A-PuroR plasmid served  
461 as the template for the standard ACE2 Kozak library containing 4096 variants using primers KAM3549  
462 and KAM3665, while the same plasmid was used to create mini libraries with primers KAM4516 and  
463 KAM3549. For generating ACE2 Kozak mutant libraries, the following plasmids and primer pairs were  
464 utilized: the I21N mutant library was created using the  
465 G868A\_AttB\_[mutATG]ACE2-I21N\_A-miRFP670\_IRES\_mCherry-H2A-P2A-PuroR plasmid with  
466 primers KAM4519 and KAM3549; the K31D mutant library was constructed using the

467 G868A\_AttB\_[mutATG]ACE2-K31D\_B-miRFP670\_IRES\_mCherry-H2A-P2A-PuroR plasmid with  
468 primers KAM4517 and KAM3549; and the D355N mutant library was generated from the  
469 G868A\_AttB\_[mutATG]ACE2-D355N\_C-miRFP670\_IRES\_mCherry-H2A-P2A-PuroR plasmid using  
470 primers KAM4518 and KAM3549. Primer sequences used for creating the sequence variant libraries  
471 can be found in **Supplementary Table 1**.

472 The following plasmids previously deposited in Addgene were used in this work:  
473 pNK005C\_BattB\_mkozak\_STIM1\_IRES\_mCherry-H2A-P2A-PuroR (Addgene plasmid #200639)  
474 (Roelle *et al*, 2023), G1088E\_pLenti-CMV-mNeonGreen -2A-HygroR (Addgene plasmid #216279)  
475 (Shukla *et al*, 2024). pMD2.G was a gift from Didier Trono (Addgene plasmid # 12259 ;  
476 <http://n2t.net/addgene:12259> ; RRID:Addgene\_12259). The SARS-CoV and SARS-CoV spike  
477 expression vectors were previously described (Shukla *et al*, 2021). Additionally, the following plasmids  
478 were deposited in Addgene as part of this work:

479 G790A\_AttB\_ACE2-miRFP670\_IRES\_mCherry-H2A-P2A-PuroR (Addgene plasmid # 237440) and  
480 G868A\_AttB\_[mutATG]ACE2-miRFP670\_IRES\_mCherry-H2A-P2A-PuroR (Addgene plasmid #  
481 237441).

482

### 483 **Genomic integration of attB plasmids into landing pad cells**

484 For the recombination of clonal ACE2-encoding attB plasmid constructs, the aforementioned  
485 HEK 293T Bxb1 landing pad cells were transfected in 6-well plates. 600,000 cells were plated into each  
486 well, and transfected with a mixture of 1.2 µg plasmid of Bxb1 attB-encoding plasmid and 5 µL of  
487 Fugene 6 transfection reagent (Promega, E2692), in 100 µL total of Opti-MEM (Gibco, 31985070).  
488 Three days after transfection, non-recombined landing pad cells were negatively selected with the  
489 addition of 10 nM AP1903 (ApexBio, B4168) to activate iCasp9. Non-silenced, recombined cells were  
490 subsequently positively selected with the addition of 1 µg/mL puromycin (InvivoGen, ANTPR1).  
491 Successfully selected cells were maintained in D10X media with 1 µg/mL puromycin to prevent  
492 transgene silencing during culture.

493 The miRFP670 Kozak library was recombined and sorted in four separate instances to create  
494 the four replicates analyzed in our dataset. For the first biological replicate, 120,000 HEK 293T cells  
495 were plated per well in a 24-well plate, and each well was transfected with a mixture of 2 µg ACE2  
496 Kozak library plasmid and 8 µL Fugene transfection reagent (Promega, E2692), diluted in 60 µL  
497 Opti-MEM (Gibco, 31985070). Eight wells were transfected per attempt and subsequently pooled. Flow  
498 cytometry analysis prior to selection showed 2.5% mCherry-positive cells, suggesting that  
499 approximately 24,000 cells were independently recombined, corresponding to an estimated 6  
500 independent events per Kozak sequence variant. Following positive and negative selection, sequencing  
501 revealed that some key Kozak sequences necessary for calibrating our results with our panel of  
502 individual variants were missing.

503 To address the coverage limitations observed in the first replicate, a modified approach was  
504 taken for the second replicate. For this replicate, 1 million cells were seeded in a 6-well plate one day  
505 before transfection. Cells were transfected with a mixture containing 4 µg ACE2 Kozak library plasmid,  
506 30 ng G790A plasmid, and 1.2 µL Xfect reagent, following the manufacturer's instructions. After  
507 positive and negative selection, approximately 8,500 cells from each of the following clonal  
508 plasmid-expressing cell lines, G1100A [TTCATCATG], G1101F [GACGACATG], G1102A  
509 [CGTCCAATG], G1103A [GCGCGCATG], G1104B [TGGTCAATG], and G1106A [TTGCACATG], were  
510 mixed with 10 million library-expressing cells to achieve a diverse range of protein abundance. For the  
511 third biological replicate, 1 million cells were seeded in a 6-well plate one day before transfection. Cells  
512 were transfected with a mixture containing 4 µg ACE2 Kozak library plasmid, 30 ng G790A plasmid and  
513 30 ng of each Kozak sequence plasmids (G1100A, G1101F, G1102A, G1103A, G1104B, and G1106A),  
514 and 1.2 µL Xfect reagent, following the manufacturer's protocol. Following recombination, cells were  
515 subjected to positive and negative selection as described before. This approach was designed to

enhance the diversity of protein abundance linked to Kozak sequence variations. For both of these replicates, ~ 170,000 cells were collected during each 4-way sort and the cells were cultured for ~48hrs before their genomic DNAs were extracted.

The fourth recombination experiment used an independent miRFP670 Kozak library, where miRFP670 was C-terminally fused to the hygromycin resistance gene. Here, cells were transfected in two separate wells of a 6-well plate using Xfect reagent. Each well containing 1 million cells was transfected with 4 µg of Hygromycin Kozak library plasmid mixed with 1.2 µL Xfect reagent. Following recombination, cells underwent positive and negative selection as mentioned above. Roughly 130,000 cells were collected in each bin during 4 way sorting and were cultured for ~48hrs before collecting them for gDNA isolation.

Additionally, each ACE2 coding variant -associated Kozak mini library was individually transfected into two separate wells of a 6-well plate using the Xfect transfection reagent (Takara Bio, 631318). Each well containing 400,000 cells was transfected with 4 µg of mini-library plasmid, mixed with 1.2 µL of Xfect reagent, following the manufacturer's protocol. The cells for each mini-library transfection were pooled prior to selection, and flow cytometry showed roughly 5% of the cells to express mCherry. Assuming each library contained 1,024 Kozak sequence variants, each Kozak mini-library is estimated to have yielded 39 independent recombination events, on average, per Kozak sequence. The library was then negatively and positively selected as described above. The separate mini-library recombinations were pooled prior to infection with pseudotyped virus.

#### **ACE2 cell surface immunofluorescence staining**

Cells expressing the original ACE2 Kozak library were trypsinized to obtain a single-cell suspension. The cell suspensions were washed with P5 buffer (PBS + 5% FBS). Cells were incubated with 1:50 dilution of ACE2 primary antibody (Abcam, ab272500) for 45 minutes at 4°C, followed by two washes with P5 buffer. Subsequently, cells were incubated with a 1:300 dilution of goat anti-rabbit IgG Alexa Fluor 488 secondary antibody (Invitrogen, A32731) for 40 minutes at 4°C in the dark. After two final washes with P5 buffer, the cells were resuspended in 200 µL of P5 buffer, and analyzed by flow cytometry.

#### **Analytical flow cytometry**

Cells were detached from the plates using trypsin, resuspended in P5 buffer, and analyzed by flow cytometry with a Thermo Fisher Attune NxT cytometer. mTagBFP2 was excited with a 405 nm laser, and emitted light was collected after passing through a 440/50 nm band pass filter. EGFP was excited with a 488 nm laser, and emitted light was collected after passing through a 530/30nm band pass filter. mCherry was excited with a 561 nm laser, and emitted light was collected after passing through a 620/15 nm band pass filter. iRFP670 and miRFP670 were excited with a 638 nm laser, and emitted light was collected after passing through a 720/30 nm band pass filter.

#### **Cell sorting by iRFP670 fluorescence**

Cells recombined with the Kozak variant libraries were sorted into 4 separate bins of gradation for near-infrared fluorescence intensity using a BD FACS ARIA SORP (BD Biosciences). mTagBFP2 was excited with a 405 nm laser, and emitted light was collected after passing through a 450/50 nm band pass filter. EGFP was excited with a 488 nm laser, and emitted light was collected after passing through a B515/20 nm band pass filter. mCherry was excited with a 561 nm laser, and emitted light was collected after passing through a 610/20 nm band pass filter. miRFP670 was excited with a 640 nm laser, and emitted light was collected after passing through a 670/30 nm band pass filter.

The pooled cell library was detached from the culture plates using Trypsin-EDTA, and subsequently transferred into D10 media. Following centrifugation at 300 x g for 3 min, the supernatants were discarded, and cell pellets were resuspended in 1 ml of cold P5 buffer. Live cells



were gated using the area values of forward and side scatter. Singlet cells were subsequently gated using the forward scatter height and area values. Recombined cells were subsequently gated by subsetting for cells with high mCherry and low mTagBFP2 fluorescence. A histogram of cell count based on iRFP670 fluorescence intensity was generated, upon which 4 gates were drawn to separate the population into quartiles. Approximately 120,000 cells were collected per bin, for 5 total replicates.

## **Pseudotyped virus infection assays**

Pseudotyped virus particles were produced in otherwise unmodified HEK 293T cells seeded into 6-well plates. Each well plated with 1 million cells was transfected with a mixture containing 1 µg of PsPax2 (Addgene #12260), 1 µg of the lentiviral transfer vector G1088E\_pLenti-CMV-mNeonGreen-2A-HygroR, and 1 µg of viral envelope plasmid (VSV-G, SARS-CoV spike, or SARS-CoV-2 spike), and PEI-Max MW 40,000 (PolySciences, CAS Number: 49553-93-7). Twelve hours after transfection, the medium was removed and the cells were washed with 1X PBS before incubating the cells with 2 mL D10 media. The viral supernatant was collected each day over the next 72 hours. For each pseudotyped virus, supernatants from nine wells of a 6-well plate were pooled. Upon collection, the media was centrifuged at 300 x g for 3 minutes, and the clarified supernatant was transferred to a fresh tube. Different volumes of clarified supernatant were used for infection: 8 mL and 24 mL for SARS1, 8 mL and 32 mL for SARS2, and 2 mL and 8 mL for VSVG. These were mixed with 6 million library cells seeded in 100 mm dishes. Four days post-infection, cells were examined under a fluorescence microscope to assess mNeonGreen expression. Subsequently, 10% of the infected library cells were harvested for genomic DNA (gDNA) isolation, while the remaining 90% were subjected to hygromycin selection (185 µg / mL and 400 µg / mL concentrations). These concentrations are much higher than normally necessarily for 293T cells, and was likely inflated due to a combination of high culture cell densities during selection, along with the presence of a large proportion of hygromycin-resistant cells within the cell population, which likely metabolized standard hygromycin concentrations, thus protecting sensitive cells at standard hygromycin concentrations (50 µg / mL). After hygromycin selection, the remaining cells were trypsinized, pelleted, and frozen for subsequent genomic DNA extraction.

## **ACE2 amplicon generation and high throughput sequencing**

Genomic DNA was isolated from each sample using the JetFlex™ Genomic DNA purification kit (Thermo Fisher, A30700). A section of DNA spanning the recombination junction, and including the Kozak sequence preceding the ACE2 open reading frame, was amplified from the genomic DNA extracts using PCR. For each 50 µL PCR reaction, the following components were used: 2 µg genomic DNA (quantified by nanodrop), 0.25 µM forward primer containing i7 index barcode and 0.25 µM reverse primer containing i5 index barcode, and 25 µL of Phusion plus high fidelity PCR mix (Thermo Fisher, F548L). A total of five PCR reactions were performed per condition, which each tube initially incubated at 95 °C for 3 minutes, followed by 25 cycles of 95 °C for 15 seconds, 60 °C for 15 seconds, 72 °C for 30 seconds, followed by a final 72 °C incubation for 1 minute. PCR products were mixed with 6x DNA loading dye (NEB, B7024S) and separated on 1.5% agarose TAE gel. Bands corresponding to the expected 293 bp amplicon size were excised and extracted using the Freeze and Squeeze kit according to the manufacturer's instructions (Bio-Rad, 7326166). Eluted PCR products were purified using a Zymo clean and concentrator kit (Zymo Research, D4003). Amplicon concentrations were measured using Qubit dsDNA BR assay kit (Life technologies, Q32853). Amplicons from all the experimental conditions were pooled in equimolar ratios and sequenced on an Illumina NextSeq550 with a 75-cycle high output kit. Oligonucleotide sequences for PCR and custom Illumina primers for sequencing are listed in **Supplementary Table 1**.

## **STIM1 Kozak library generation and cell survival assay**

613 The STIM1 Kozak library was generated using an oligonucleotide primer (Integrated DNA  
614 technologies) where the -6 to -1 nucleotides preceding the STIM1 start codon was encoded by a  
615 degenerate XNNNNN segment, where X is the invariant nucleotide at the -6 position for barcoding (A  
616 for WT, C for R429C, and G for R304W) (**Fig 7A, 7D**). Gibson cloning, electroporation, and individual  
617 library purification was performed as described for ACE2, above. The three plasmid libraries were  
618 individually prepared, subsequently mixed in equimolar ratios, and transformed into DH10 $\beta$  *E.coli*,  
619 which was midprepped to yield the final library introduced into the landing pad cells.

620 For each replicate, two 100 mm plates, each with 3.5 million HEK 293T landing pad cells, were  
621 transfected with the plasmid library using the Xfect transfection reagent, as described above. Cells  
622 were harvested 5, 7, and 9 days following transfection. Genomic DNA was extracted from each time  
623 point using DNeasy Blood and Tissue Kit (Qiagen, 69506), and quantitated with a Qubit fluorometer  
624 using the Qubit Broad Range dsDNA DNA quantification kit (Thermo Fisher, Q32853).

625 Both the midprepped plasmid library, as well as the genomic DNA from each time-point, were  
626 amplified by PCR to create the material necessary for high throughput DNA sequencing. The reaction  
627 conditions were similar to that of ACE2, except 200 ng of genomic DNA (as quantified by the broad  
628 range dsDNA Qubit kit) was used as the starting material. Amplicons were separated on a 1.5%  
629 agarose TAE gel, excised, extracted, and quantitated by broad range dsDNA Qubit as described above.  
630 The vast majority of samples were sequenced on an Illumina NextSeq 550 using a Mid Output 150  
631 cycle kit by the CWRU Genomics Core. The first three replicates of the STIM1 Kozak library were  
632 sequenced using the Illumina MiSeq, generated through submission to the Amplicon-EZ service offered  
633 by Genewiz / Azenta. Oligonucleotide sequences for PCR and custom Illumina primers for sequencing  
634 are listed in **Supplementary Table 1**.

635

#### 636 **Identification of clinical germline Kozak variants**

637 The current list of reference sequence identifiers for GRCh38 was downloaded from NCBI. The  
638 reference RNA sequences were translated and cross referenced with the reference protein sequences  
639 for each gene to identify the first exact protein match, and the 6 nucleotide positions preceding the start  
640 codon in the RNA were returned as the Kozak sequence. As a secondary approach, the longest  
641 possible translated protein sequence was identified for each RNA, and if a methionine was present, the  
642 6 nucleotides preceding the first methionine were used to identify the Kozak sequence.

643 The March 2025 release of ClinVar was used to identify observed clinical variants that occur  
644 within the Kozak sequence. The data was isolated to the GRCh38 assembly to match the reference  
645 sequences, and entries were filtered for variants between position -6 and position -1. Kozak sequence  
646 variants that overlapped with introns were identified by the script, but not used for subsequent analysis  
647 due to possible additional complications of transcript splicing. Kozak variant sequences were then  
648 paired with the associated RNA sequence using the NM accession. The variant was then checked  
649 against the Kozak generated by the first method and applied if a positional match was found, and both  
650 the original and new sequence were returned. If the first method generating the Kozak returned no  
651 sequence, or if the positional mutation did not match the generated Kozak, then the Kozak returned by  
652 the second method was used instead, and the variant was returned using that approach instead.  
653 Variants involving microsatellites were ignored in this analysis. 1,826 explicit Kozak variants were  
654 identified from the 2,558 total variants within the Kozak region identified in the ClinVar database  
655 (**Supplementary Table 2**).

656

#### 657 **Data analysis**

658 For short-read sequencing generated by the Illumina NextSeq, the forward and reverse reads  
659 were paired using PEAR (Zhang *et al*, 2014). Kozak sequences were counted from the paired reads  
660 using Enrich2 (Rubin *et al*, 2017), and filtered to exclude reads possessing nucleotides with quality  
661 scores less than 20. For longer-read sequencing generated by the Illumina MiSeq, generated through

submission to the Amplicon-EZ service offered by Genewiz / Azenta, the reads were paired as above, except the paired reads were subsequently processed with a custom Python script “Extract\_Kozak.py”, which identified true Kozak library reads from template molecule reads, and for each Kozak read, extracted the Kozak sequence found in that read. All subsequent analyses of the sequencing outputs were performed in R version 4.3.1 (2023-06-16). An R markdown file with code to recreate the analysis (Kozak.Rmd), along with the relevant data files and the various python scripts for the initial processing of FASTQ files, can be found in the MatreyekLab Github repository under “MatreyekLab/Kozak”. A table of the fastq files generated and analyzed for this work is included as **Supplementary Table 3**.

The Kozak sort-seq scores were calculated similarly to previous work (Matreyek *et al*, 2018, 2021), with some minor changes. For samples sequenced to sufficient read depth, a density-plot of sequence counts normally yields a bimodal distribution, with one peak stemming from a log-normal distribution of counts with a median of 10 or greater, largely reflecting sequences of physical molecules amplified and sequenced from the sample, and a separate peak with a count of 1, largely reflecting sequences derived from sequencing error. We harnessed this property to computationally remove erroneous sequence counts. For each bin, we identified the local minima between these two peaks, and removed sequence counts below this sample-specific threshold value, to yield a dataset of filtered counts.

For each sequenced sample, the filtered count of each variant was divided by the sum of counts recorded in that sample to obtain variant-specific frequencies ( $F_{v,bin}$ ). For replicates 1 and 2, which both included separately sequenced amplification “technical” replicates derived from the same sorted genomic DNA, the technical replicate frequencies were averaged to yield an average frequency for each variant, which was used as the  $F_{v,bin}$  value. These frequencies were used to calculate a weighted average for each variant for each replicate ( $W_{v,rep}$ ), using the following formula.

685

$$W_{v,rep} = \frac{(F_{v,bin1} \times 0) + (F_{v,bin2} \times (1/3)) + (F_{v,bin3} \times (2/3)) + (F_{v,bin4} \times 1)}{F_{v,bin1} + F_{v,bin2} + F_{v,bin3} + F_{v,bin4}}$$

687

Thus, all weighted average values ranged from a value of 0 to 1. Pairwise comparisons of variant-specific weighted averages are shown in **Supplementary Fig 2**. Once the weighted average values were calculated for each variant for each replicate, they were  $\log_{10}$  transformed, averaged, and the base-10 exponential calculated to yield the geometric mean weighted average value. Correspondingly, the standard deviation of the  $\log_{10}$  transformed values were calculated and used to calculate the upper and lower 95% confidence intervals, which were later transformed as a base-10 exponential to accompany the geometric mean weighted averages.

To calibrate these weighted averages to MFI equivalent values, we generated cells recombined with ACE2-miRFP670 constructs encoding 16 different Kozak sequences, which were measured for miRFP670 fluorescence intensity using analytical flow cytometry. A linear model was first generated to establish the conversion factor enabling scaling of our weighted average scores to MFI-equivalent values. While accurate for values between 1% and 100% of the consensus Kozak, the linear model performed poorly for extremely high or low values, with the minimum and maximum scaled values being 0.0003 and 3.89; both of these values were outside of the range physically observed with this assay. We thus used logistic regression to approximate the linear model, but furthermore bound all scaled values between 0.004 and 1.34. These resulting values are referred to as the calibrated scores. These scores are provided in **Supplementary Table 4**.

Enrichment values for infection experiments were initially filtered similarly to the sort-seq scores, wherein we identified the local minima between the two peaks observed in a density plot representation of sequence counts, and removed sequence counts below his sample-specific threshold value, to yield a dataset of filtered counts. The counts for each variant were divided by the total counts for that sequence sample, to yield sample-specific variant frequencies. For infection samples that included

separately sequenced amplification “technical” replicates derived from the same sorted genomic DNA, the geometric means of the technical replicate frequencies were used. Each hygromycin-selected infected sample had a corresponding unselected sample. For each pair, we divided variant-specific frequencies following selection by those prior to selection, obtaining an enrichment ratio. The STIM1 survival scores were calculated similarly, with the exception that the ratio was the quotient of each Kozak variant frequency recombined into cells divided by the frequency of that variant in the sequenced plasmid library. The scores for these functional assays are found in **Supplementary Tables 4 and 5**.

## Acknowledgements

The authors wish to thank Simone Edelheit and Milena Zelembaba of the Genomics Core Facility of the CWRU School of Medicine’s Genetics and Genome Sciences Department. The Cytometry & Imaging Microscopy Shared Resource of the Case Comprehensive Cancer Center was supported by NIH grants P30CA043703 and S10OD021559. Nidhi Shukla thanks the Flora Stone Mather Center for Women at CWRU for providing a research and professional development grant to support the presentation of this work at the Discover BMB 2023 conference.

## Data Availability

The authors affirm that all data necessary for confirming the conclusions of the article are present within the article, figures and tables. Key plasmids have been deposited to and available via Addgene. Code to recreate analysis is available on Github (<https://github.com/MatreyekLab/Kozak>). Raw FASTQ data can be found at the NCBI GEO repository under accession number GSE295498.

## Competing interests

The authors declare that no competing interests exist.

## Funding

Funder	Grant reference Number	Author
National Institutes of Health	GM142886	Kenneth A Matreyek
National Institutes of Health	AI178151	Kenneth A Matreyek
National Institutes of Health	AI161275	Anna M Bruchez

The funders had no role in study design, data collection and interpretation, or the decision to submit the work for publication.

## Author contributions

Nidhi Shukla: Investigation, Methodology, Writing - review and editing  
Nisha D Kamath: Investigation, Methodology, Writing - review and editing  
John C Snell: Investigation, Data curation, Formal analysis, Methodology, Writing - review and editing  
Anna M Bruchez: Writing - review and editing  
Kenneth A Matreyek: Conceptualization, Methodology, Investigation, Data curation, Formal analysis, Visualization, Writing - review and editing, Supervision, Funding acquisition, Methodology, Project administration.

## Author ORCIDs

Nidhi Shukla <https://orcid.org/0000-0001-5912-7039>  
Nisha D Kamath <https://orcid.org/0000-0001-8969-0631>  
John C Snell <https://orcid.org/0000-0003-2683-6108>  
Anna M Bruchez <https://orcid.org/0000-0003-1695-5349>  
Kenneth A Matreyek <https://orcid.org/0000-0001-9149-551X>



760 **Bibliography:**

- 761 Acevedo JM, Hoermann B, Schlombach T & Teleman AA (2018) Changes in global translation  
762 elongation or initiation rates shape the proteome via the Kozak sequence. *Sci Rep* 8: 4018
- 763 Ambrosini C, Destefanis E, Kheir E, Broso F, Alessandrini F, Longhi S, Battisti N, Pesce I, Dassi E,  
764 Petris G, *et al* (2022) Translational enhancement by base editing of the Kozak sequence rescues  
765 haploinsufficiency. *Nucleic Acids Res* 50: 10756–10771
- 766 Bhattacharjee MJ, Lin J-J, Chang C-Y, Chiou Y-T, Li T-N, Tai C-W, Shiu T-F, Chen C-A, Chou C-Y,  
767 Chakraborty P, *et al* (2021) Identifying primate ACE2 variants that confer resistance to  
768 SARS-CoV-2. *Mol Biol Evol* 38: 2715–2731
- 769 De Angioletti M, Lacerra G, Sabato V & Carestia C (2004) Beta+45 G --> C: a novel silent  
770 beta-thalassaemia mutation, the first in the Kozak sequence. *Br J Haematol* 124: 224–231
- 771 Farrell AG, Dadonaite B, Greaney AJ, Eguia R, Loes AN, Franko NM, Logue J, Carreño JM, Abbad A,  
772 Chu HY, *et al* (2022) Receptor-Binding Domain (RBD) Antibodies Contribute More to SARS-CoV-2  
773 Neutralization When Target Cells Express High Levels of ACE2. *Viruses* 14
- 774 Johnston SH, Lobritz MA, Nguyen S, Lassen K, Delair S, Posta F, Bryson YJ, Arts EJ, Chou T & Lee B  
775 (2009) A quantitative affinity-profiling system that reveals distinct CD4/CCR5 usage patterns  
776 among human immunodeficiency virus type 1 and simian immunodeficiency virus strains. *J Virol*  
777 83: 11016–11026
- 778 Kamath ND & Matreyek KA (2025) Comprehensive mutational characterization of the calcium-sensing  
779 STIM1 EF-hand reveals residues essential for structure and function. *bioRxiv*
- 780 Kozak M (1981) Possible role of flanking nucleotides in recognition of the AUG initiator codon by  
781 eukaryotic ribosomes. *Nucleic Acids Res* 9: 5233–5252
- 782 Kozak M (1986) Point mutations define a sequence flanking the AUG initiator codon that modulates  
783 translation by eukaryotic ribosomes. *Cell* 44: 283–292
- 784 Kozak M (1987) At least six nucleotides preceding the AUG initiator codon enhance translation in  
785 mammalian cells. *J Mol Biol* 196: 947–950
- 786 Kozak M (1989) The scanning model for translation: an update. *J Cell Biol* 108: 229–241
- 787 Kristensen AR, Gsponer J & Foster LJ (2013) Protein synthesis rate is the predominant regulator of  
788 protein expression during differentiation. *Mol Syst Biol* 9: 689
- 789 Landrum MJ, Lee JM, Benson M, Brown GR, Chao C, Chitipiralla S, Gu B, Hart J, Hoffman D, Jang W,  
790 *et al* (2018) ClinVar: improving access to variant interpretations and supporting evidence. *Nucleic*  
791 *Acids Res* 46: D1062–D1067
- 792 Matoy EJ, Plowman JN, Watson CJ, Belshan MA, Blue EE, Huff CD & Stessman HAF (2024) In vitro  
793 data suggest a role for PMS2 Kozak sequence mutations in Lynch syndrome risk. *HGG Adv* 5:  
794 100298
- 795 Matreyek KA, Starita LM, Stephany JJ, Martin B, Chiasson MA, Gray VE, Kircher M, Khechaduri A,  
796 Dines JN, Hause RJ, *et al* (2018) Multiplex assessment of protein variant abundance by massively  
797 parallel sequencing. *Nat Genet* 50: 874–882
- 798 Matreyek KA, Stephany JJ, Ahler E & Fowler DM (2021) Integrating thousands of PTEN variant activity  
799 and abundance measurements reveals variant subgroups and new dominant negatives in cancers.  
800 *Genome Med* 13: 165

801 Matreyek KA, Stephany JJ, Chiasson MA, Hasle N & Fowler DM (2020) An improved platform for  
802 functional assessment of large protein libraries in mammalian cells. *Nucleic Acids Res* 48: e1

803 Matreyek KA, Stephany JJ & Fowler DM (2017) A platform for functional assessment of large variant  
804 libraries in mammalian cells. *Nucleic Acids Res* 45: e102

805 Miller DT, Lee K, Abul-Husn NS, Amendola LM, Brothers K, Chung WK, Gollob MH, Gordon AS,  
806 Harrison SM, Hershberger RE, *et al* (2023) ACMG SF v3.2 list for reporting of secondary findings  
807 in clinical exome and genome sequencing: A policy statement of the American College of Medical  
808 Genetics and Genomics (ACMG). *Genet Med*: 100866

809 Mohan RA, van Engelen K, Stefanovic S, Barnett P, Ilgun A, Baars MJH, Bouma BJ, Mulder BJM,  
810 Christoffels VM & Postma AV (2014) A mutation in the Kozak sequence of GATA4 hampers  
811 translation in a family with atrial septal defects. *Am J Med Genet A* 164A: 2732–2738

812 Noderer WL, Flockhart RJ, Bhaduri A, de Arce AJD, Zhang J, Khavari PA & Wang CL (2014)  
813 Quantitative analysis of mammalian translation initiation sites by FACS-seq. *Mol Syst Biol* 10

814 Petersen SD, Zhang J, Lee JS, Jakočiūnas T, Grav LM, Kildegaard HF, Keasling JD & Jensen MK  
815 (2018) Modular 5'-UTR hexamers for context-independent tuning of protein expression in  
816 eukaryotes. *Nucleic Acids Res* 46: e127–e127

817 Ren W, Zhu Y, Lan J, Chen H, Wang Y, Shi H, Feng F, Chen D-Y, Close B, Zhao X, *et al* (2022)  
818 Susceptibilities of human ACE2 genetic variants in Coronavirus infection. *J Virol* 96: e0149221

819 Roelle SM, Kamath ND & Matreyek KA (2023) Mammalian Genomic Manipulation with Orthogonal  
820 Bxb1 DNA Recombinase Sites for the Functional Characterization of Protein Variants. *ACS Synth*  
821 *Biol* 12: 3352–3365

822 Roelle SM, Shukla N, Pham AT, Bruchez AM & Matreyek KA (2022) Expanded ACE2 dependencies of  
823 diverse SARS-like coronavirus receptor binding domains. *PLoS Biol* 20: e3001738

824 Rubin AF, Gelman H, Lucas N, Bajjalieh SM, Papenfuss AT, Speed TP & Fowler DM (2017) A statistical  
825 framework for analyzing deep mutational scanning data. *Genome Biol* 18: 150

826 Shukla N, Roelle SM, Snell JC, DeSignore O, Bruchez AM & Matreyek KA (2024) Pseudotyped virus  
827 infection of multiplexed ACE2 libraries reveals SARS-CoV-2 variant shifts in receptor usage. *PLoS*  
828 *Pathog* 20: e1012044

829 Shukla N, Roelle SM, Suzart VG, Bruchez AM & Matreyek KA (2021) Mutants of human ACE2  
830 differentially promote SARS-CoV and SARS-CoV-2 spike mediated infection. *PLoS Pathog* 17:  
831 e1009715

832 Starita LM, Ahituv N, Dunham MJ, Kitzman JO, Roth FP, Seelig G, Shendure J & Fowler DM (2017)  
833 Variant interpretation: Functional assays to the rescue. *Am J Hum Genet* 101: 315–325

834 Xie J, Zhuang Z, Gou S, Zhang Q, Wang X, Lan T, Lian M, Li N, Liang Y, Ouyang Z, *et al* (2023)  
835 Precise genome editing of the Kozak sequence enables bidirectional and quantitative modulation  
836 of protein translation to anticipated levels without affecting transcription. *Nucleic Acids Res* 51:  
837 10075–10093

838 Zhang J, Kobert K, Flouri T & Stamatakis A (2014) PEAR: a fast and accurate Illumina Paired-End reAd  
839 mergeR. *Bioinformatics* 30: 614–620